New Structural Characterization of the $Li_xV_2O_5$ System Provided by Raman Spectroscopy

R. Baddour-Hadjean,*,† E. Raekelboom,‡ and J. P. Pereira-Ramos‡

Laboratoire de Dynamique, Interactions et Réactivité (LADIR), UMR 7075 CNRS et Université Pierre et Marie Curie, 2 rue Henri Dunant, 94320 Thiais, France, and Laboratoire d'Electrocatalyse et Synthèse Organique, UMR 7582 CNRS et Université Paris XII, 2 rue Henri Dunant, 94320 Thiais, France

Received March 6, 2006. Revised Manuscript Received April 25, 2006

The Raman spectra of the ϵ-, δ-, and γ-$Li_xV_2O_5$ powdered phases are reported. New fingerprints are obtained and discussed in connection with those previously reported for electrochemically and chemically lithiated V_2O_5. The metastable character of the δ-phase is explored through the XRD and Raman study of the $\delta \rightarrow \epsilon \rightarrow \gamma$ "high temperature" phase transitions and allows explaining the great disparities encountered in the literature spectra. The knowledge of these reference Raman spectra for the $Li_xV_2O_5$ phases constitutes fundamental data for understanding the electrochemical cycling behavior of the Li/V_2O_5 system.

Introduction

Vanadium pentoxide has been the subject of numerous studies devoted to its capacity to accommodate lithium ions according to the electrochemical reaction $V_2O_5 + xLi^+ + xe^- \Leftrightarrow Li_xV_2O_5$.[1−2] Technological applications of this property can be found in electrochromic thin film devices and batteries.[3−6]

Nevertheless, despite all the efforts devoted to the study of the lithium insertion process in V_2O_5, the system is far from being completely elucidated, and this is principally due to the complex nature of the lithiated phases occurring during the cycling processes. Depending on the amount of lithium (x) intercalated in V_2O_5, several structural modifications have been reported.[1,6−10] Considering the bulk material, the α-, ϵ-, and δ-$Li_xV_2O_5$ were identified from the above reaction in the $0 < x \leq 1$ composition range. The α-$Li_xV_2O_5$ phase occurs with $x < 0.1$. The ϵ-phase exists in the range $0.3 < x < 0.7$, and the δ-phase appears with x between 0.9 and 1. The lithium content corresponding to the limiting composition of the three solid solutions differs slightly from one report to another. All these phase transitions are fully reversible in this composition range, and the structure of the pristine V_2O_5 phase is recovered upon deintercalation. The situation becomes more problematic for lithium contents larger than one, the δ-phase being transformed into a γ one via an irreversible reconstruction mechanism.[6] The γ-phase structure remains stable even after deintercalation of all Li atoms,[6] leading to a new metastable γ' variety of V_2O_5.[11] More recently, it has been reported that the intercalation of three lithium ions in V_2O_5 was possible through the formation of a weakly crystallized cubic phase, namely, ω-$Li_3V_2O_5$.[12] However, some authors put in doubt the Li/V_2O_5 phase diagram for $x > 1$, reporting the appearance of a mixture of Li_xVO_2 and Li_3VO_4 compounds instead of the so-called "γ-" and "ω-phases".[13]

Considering the case of V_2O_5 films, several studies carried out on polycrystalline films seem to show that the structural features of the lithiated phases can significantly vary depending on the synthesis conditions.[14−18] In situ XRD experiments performed on sol−gel derived $Li_xV_2O_5$ films have reported notable differences in the structural evolution for $x > 0.4$ as compared to other films and powders, namely, the existence of an unexpected elongated c axis for $x = 0.8$ as well as the nonappearance of the δ-phase usually described for $x = 1$.[17] More recently, some of us have shown that the structural response of crystalline V_2O_5 films prepared by direct current sputtering differs from that known for bulk V_2O_5 powders.[18]

* To whom correspondence should be addressed. E-mail: baddour@glvt-cnrs.fr.
† Université Pierre et Marie Curie.
‡ Université Paris XII.

(1) Murphy, D. W.; Christian, P. A.; Disalvo, F. J.; Waszczak, J. V. *Inorg. Chem.* **1979**, *18*, 2800.
(2) Whittingham, M. S. *J. Electrochem. Soc.* **1976**, *126*, 315.
(3) Wiesener, K.; Shneider, W.; Ilic, D.; Steger, E.; Hallmeir, K. H.; Brackmann, E. *J. Power Sources* **1978**, *20*, 157.
(4) Livage, J. *Chem. Mater.* **1991**, *3*, 578.
(5) Bates, J. B.; Gruzalski, G. R.; Dudney, N. J.; Luck, C. F.; Xiaohua, Y. *Solid State Ionics* **1994**, *70/71*, 619.
(6) Cocciantelli, J. M.; Doumerc, J. P.; Pouchard, M.; Broussely, M.; Labat, J. *J. Power Sources* **1991**, *34*, 103.
(7) Dickens, P. G.; French, S. J.; Hight, A. T.; Pye, M. F. *Mater. Res. Bull.* **1979**, *14*, 1295.
(8) Galy, J.; Darriet, J.; Hagenmuller, P. *Rev. Chim. Miner.* **1971**, *8*, 509.
(9) Rozier, P.; Savariault, J.-M.; Galy, J.; Marichal, C.; Horschinger, J.; Granger, P. *Eur. J. Solid State Inorg. Chem.* **1996**, *33*, 1.
(10) Galy, J. *J. Solid State Chem.* **1992**, *100*, 229.
(11) Cocciantelli, J. M.; Gravereau, J. M.; Doumerc, J. P.; Pouchard, M.; Hagenmuller, P. *J. Solid State Chem.* **1991**, *93*, 497.
(12) Delmas, C.; Brethes, S.; Ménétrier, M. *J. Power Sources* **1991**, *34*, 113.
(13) Rozier, P.; Savariaut, J. M.; Galy, J. *Solid State Ionics* **1997**, *98*, 133.
(14) Talledo, A.; Granqvist, C. G. *J. Appl. Phys.* **1995**, *77*, 4655.
(15) Ptitsyn, M. V.; Tikhonov, K. I.; Rotinyan, A. L. *Sov. Electrochem.* **1981**, *17*, 1297.
(16) Andrukaitis, E.; Jacobs, P. W. M.; Lorimer, J. W. *Solid State Ionics* **1988**, *27*, 19.
(17) Meulenkamp, E. A.; van Klinken, W.; Schlatmann, A. R. *Solid State Ionics* **1999**, *126*, 235.
(18) Navone, C.; Pereira-Ramos, J. P.; Salot, R.; Baddour-Hadjean, R. *J. Electrochem. Soc.* **2005**, *152*, 1790.

10.1021/cm060540g CCC: $33.50
Published on Web 07/01/2006

In particular, powder X-ray diffraction (XRD) experiments have evidenced a single phase behavior in the $0 < x \leq 1$ lithium content range. Surprisingly, a ϵ-related phase has been shown to exist in a wide composition range $0.3 < x \leq 1$, and the δ-phase has not been detected. Moreover, the γ-phase is never found for higher lithium contents.

Such widely different findings with regard to the structural response require the knowledge of specific fingerprints for the different $Li_xV_2O_5$ phases involved during the electrochemical process. A number of structural investigations on the $Li_xV_2O_5$ system were carried out using different experimental techniques such as XRD,[9,13,17] X-ray absorption,[19] NMR,[20] electron paramagnetic resonance,[21] and neutron and electron diffraction.[22−24] Raman spectroscopy on the other hand seems to be quite promising for this purpose because determination of frequencies of normal vibrations provides a very sensitive tool to detect the local structure variations. However, very few studies are devoted to the Raman features of the $Li_xV_2O_5$ phases.[25−29] This is probably due to the fact that efficiency of the Raman spectroscopy study depends on the availability of a credible band assignment. This requires reference spectra for the different $Li_xV_2O_5$ phases which are formed during the discharge of the cell. A previous ex situ Raman study of V_2O_5 before and after electrochemical Li insertion concluded to a fast amorphization of the oxide:[25] the V_2O_5 lines vanish nearly completely after discharge, and only weak intensities are recovered during the charge. A preliminary confocal Raman microspectrometry study reports for the first time that it is possible to follow in situ the spectral changes of vanadium oxide in a composite cathode of a working lithium battery with a solid polymer electrolyte.[28] However, reference Raman spectra of the different $Li_xV_2O_5$ phases were difficult to obtain in this configuration because of the Li concentration gradient within the composite electrode. More recently, our ex situ Raman investigations carried out on V_2O_5 polycrystalline films synthesized by atomic layer deposition have allowed for the first time high quality Raman spectra in a wide lithium composition range ($0 < x < 1$) to be obtained, particularly due to the high homogeneity of the lithium insertion process in the pure thin film of oxide.[29] Specific Raman fingerprints were reported for the electrochemically lithiated α-, ϵ-, and δ-$Li_xV_2O_5$ phases occurring for $x < 1$. However, these spectra differ significantly from those previously reported for the chemically formed $Li_xV_2O_5$ phases.[26] It must be outlined that ref 26 deals with high temperature lithiated phases reported as being ϵ- and γ-LiV_2O_5 obtained from heat treatments of the chemically prepared δ-LiV_2O_5. In particular, the ϵ-related phase ϵ-LiV_2O_5 has no electrochemical equivalent.

Here we report the Raman spectra obtained for the ϵ-, δ-, and γ-$Li_xV_2O_5$ powders synthesized through chemical reactions. New Raman fingerprints are obtained and discussed in connection with those previously reported for electrochemically and chemically lithiated V_2O_5. The metastable character of the δ-phase is explored through the study of the $\delta \rightarrow \epsilon \rightarrow \gamma$ "high temperature" phase transitions and allows explaining the great disparities encountered in the literature spectra.

Experimental Section

Materials. Low temperature $Li_xV_2O_5$ ($x \leq 1$) phases can be obtained by soft chemistry through the following chemical insertion reaction:[1]

$$V_2O_5 + x\text{LiI (in } CH_3CN) \leftrightarrow Li_xV_2O_5 + (x/2)I_2$$

Twophases, ϵ- and δ-$Li_xV_2O_5$, were prepared from the above reaction, by reacting V_2O_5 with an excess of LiI in acetonitrile (excess of 70% used to obtain the expected stoichiometric $Li_xV_2O_5$). The mixture was stirred for several days at room temperature to obtain the ϵ-phase and at 50 °C for the δ-phase. The products of the reaction were isolated by filtration, washed in acetonitrile, and dried in air. Chemical analyses of Li by inductively coupled plasma atomic absorption spectroscopy indicate 0.52 and 1 Li/mol of V_2O_5 for the ϵ- and δ-phase, respectively. Further coulometric titration experiments allow these results to be confirmed and the following compositions for the ϵ- and δ-phases to be checked: ϵ-$Li_{0.52}V_2O_5$ and δ-LiV_2O_5.

Samples of γ-$Li_xV_2O_5$ phases were prepared via two routes according to the following procedures:

(a) The first route includes heating in air the chemically prepared δ-phase. Indeed, previous works report that δ-LiV_2O_5 can be irreversibly transformed to γ-LiV_2O_5 above 200 °C.[1,10,30] The heat treatment applied here to the δ-phase consisted of an increase of temperature at a rate of 2°/min followed by a 10 h plateau at 250 °C and a decrease at 20°/min until the room temperature is reached. The corresponding γ-LiV_2O_5 sample is called γ_{th}.

(b) Chemical lithiation attempts have been performed to get the highest lithium content allowed in the $Li_xV_2O_5$ system.[7] We used *n*-butyllithium as reducing agent, added to a V_2O_5 solution in pentane with an initial ratio $Li/V_2O_5 = 2$. The product was washed with dry pentane and dried in air. From the faradic yield achieved during the course of the electrochemical oxidation, the lithium content in this sample is estimated to be of about 1.3 Li/mol. The corresponding as-prepared lithium-rich product is called the LR phase.

Methods. XRD patterns were recorded with a Bruker D8 Advance diffractometer with the Cu Kα radiation scanning between 10 and 80° by steps of 0.02° (2θ) with a fixed counting times of 8 s. The Rietveld structure refinement was performed using the Fullprof program.

The Raman spectra were recorded at room temperature using a micro-Raman system with a Labram spectrometer including a charge-coupled device detector. A frequency doubled Nd:YAG laser operating at 532 nm was used as the excitation source. The spectra

(19) Prouzet, E.; Cartier, C.; Vilain, F.; Tranchant, A. *J. Chem. Soc., Faraday Trans.* **1996**, *92*, 103.
(20) Hirschinger, J.; Mongrelet, T.; Marichal, C.; Granger, P.; Savariault, J. M.; Déramond, E.; Galy, J. *J. Phys. Chem.* **1993**, *97*, 10301.
(21) Pecquenard, B.; Gourier, D.; Baffier, N. *Solid State Ionics* **1995**, *78*, 287.
(22) Cava, R. J.; Santoro, A.; Murphy, D. W.; Zahurak, S. M.; Fleming, R. M.; Marsh, P.; Roth, R. S. *J. Solid State Chem.* **1986**, *65*, 63.
(23) Savariault, J. M.; Rozier, P. *Physica B* **1997**, *234−236*, 97.
(24) Katzke, H.; Czank, M.; Depmeier W.; Van Smaale, S. *Philos. Mag. B* **1997**, *75*, 757.
(25) Cazzanelli, E.; Mariotto, G.; Passerini, S.; Decker, F. *Solid State Ionics* **1994**, *70/71*, 412.
(26) Zhang, X.; Frech, R. *Electrochim. Acta* **1997**, *42*, 475.
(27) Zhang, X.; Frech, R. *J. Electrochem. Soc.* **1998**, *145*, 847.
(28) Rey, I.; Lassègues, J. C.; Baudry, P.; Majastre, H. *Electrochim. Acta* **1998**, *43*, 1539.
(29) Baddour-Hadjean, R.; Golabkan, V.; Pereira-Ramos, J. P.; Mantoux, A.; Lincot, D. *J. Raman Spectrosc.* **2002**, *33*, 631.
(30) Satto, C.; Sciau, P.; Dooryhee, E.; Galy, J.; Millet, P. *J. Solid State Chem.* **1999**, *146*, 103.

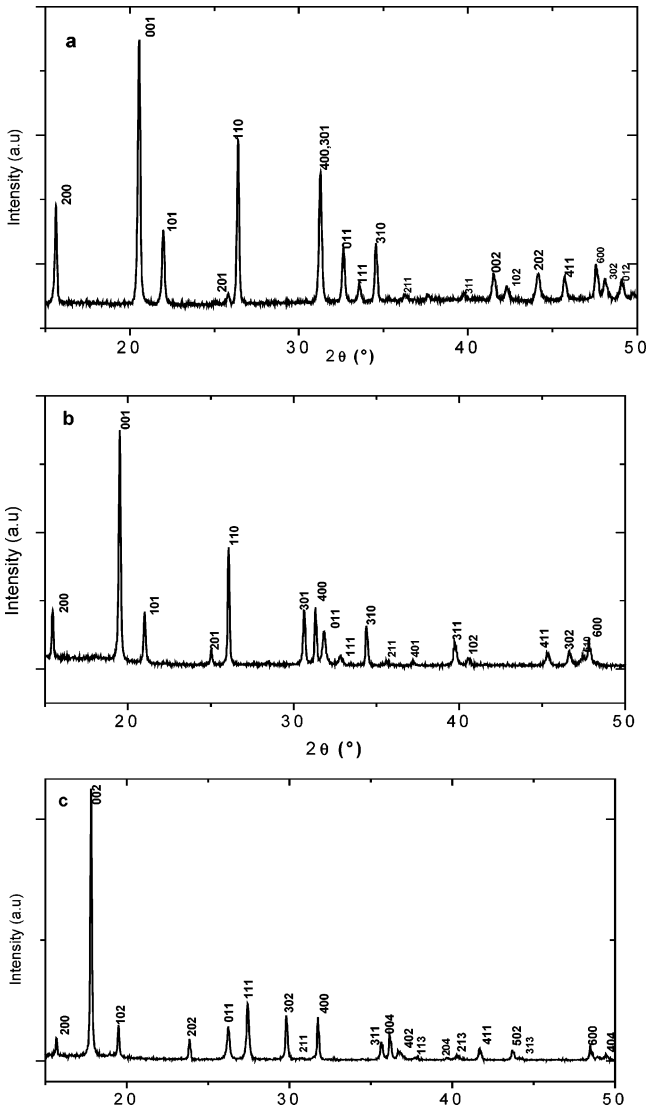

Figure 1. XRD patterns of α-V_2O_5 (a) chemically prepared ϵ-$Li_{0.52}V_2O_5$ (b) and δ-LiV_2O_5 (c).

Table 1. Lattice Parameters and Cell Volumes for α-V_2O_5, ϵ-$Li_{0.52}V_2O_5$, and δ-LiV_2O_5 Phases

	α-V_2O_5 (*Pmmn*)	ϵ-phase (*Pmmn*)	δ-phase (*Amma*)
a (Å)	11.5120(1)	11.3840 (4)	11.2429 (2)
b (Å)	3.5642(1)	3.5662 (1)	3.6026 (1)
c (Å)	4.3685(4)	4.5251 (1)	9.9113 (3)
V/*Z* (Å^3)	89.6	91.85	100.36

were measured in backscattering geometry. The resolution was about 0.5 cm^{-1}. A 100× objective was used to focus the laser light on sample surface to a spot size of 1 μm^2, and the laser power was kept to 0.2 mW to avoid any degradation of the electrode.

Results and Discussion

Structural Study of the δ-, ϵ-, and LR phases. As shown in Figure 1, the XRD patterns for the chemically prepared ϵ-$Li_{0.52}V_2O_5$ and δ-LiV_2O_5 phases are typical of well-crystallized samples. The corresponding space groups and refined lattice parameters (Table 1) are consistent with previous structural data.[1,7,10,22] The structures of the vanadium−oxygen layers are rather similar in pure V_2O_5 and in α-, ϵ-, and δ-phases of $Li_xV_2O_5$ (see Figure 2a−c), with, however, an increased puckering of the layers revealed by the decrease

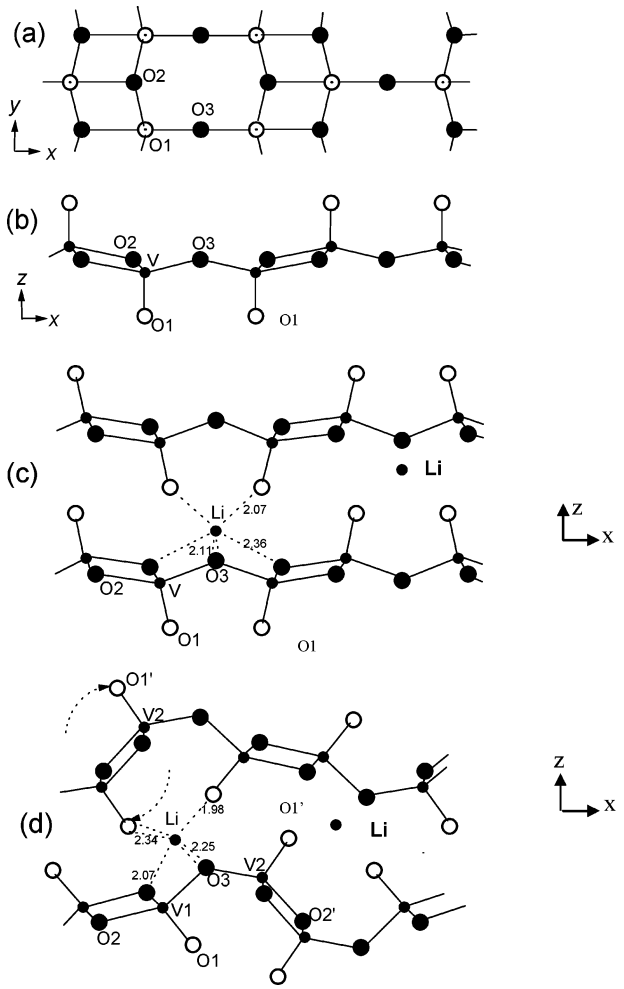

Figure 2. Crystal structure of α-V_2O_5 in the *xy* (a) and in the *xz* projection (b); crystal structure of δ-LiV_2O_5 (c) and γ-LiV_2O_5 in the *xz* projection (d).

in the *a* parameter. Moreover, the increase of the number of inserted lithium ions between the layers is responsible for the increase in the *c* parameter. The local environment of the vanadium atom in V_2O_5 leads to the existence of four types of vanadium−oxygen bonds[31] (V−O bond lengths d_1 to d_4 vary from 1.58 to 2.02 Å): short and strong V═O1 bonds oriented along the *c* axis (d_1 = 1.5848 Å), bridge V−O3 bonds (d_2 = 1.7798 Å), and interchain V−O2 bonds (d_3 = 1.8777 Å and d_4 = 2.0206 Å).

In δ-LiV_2O_5, the layers are much more puckered[22] (*a* parameter still decreases to reach the value of 11.243 Å), and a shift of every second layer in the *y* direction on *b*/2 is observed. This means that the elementary unit cell of the δ-LiV_2O_5 phase is doubled in the *z* direction and becomes base-centered (space group *Amma* or D_{2h}^{17}).

Figure 3a shows the XRD pattern of the as-prepared LR sample obtained through chemical lithiation of V_2O_5 with *n*-butyllithium. Even though the refinement is hampered by the low crystallinity of the sample, the data analysis seems to show the presence of both δ− (space group *Amma*, *a* = 11.23 Å, *b* = 3.61 Å, and *c* = 9.90 Å) and γ-phases (space group *Pnma*, *a* = 9.98 Å, *b* = 3.65 Å, and *c* = 10.59 Å). The XRD pattern of the heat-treated LR phase at 400 °C

(31) Enjalbert, R.; Galy, J. *Acta Crystallogr., Sect. C* **1986**, *42*, 1467.

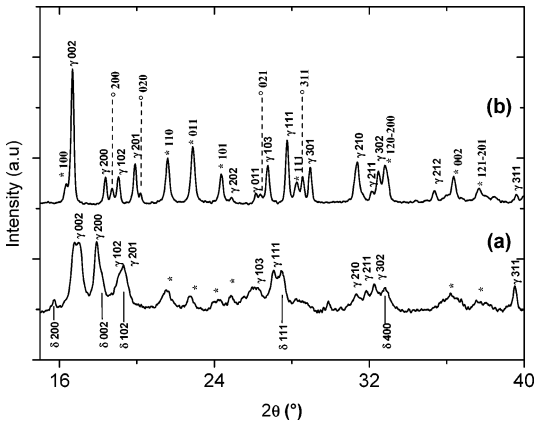

Figure 3. XRD patterns of the chemically prepared LR phase (a) and after annealing treatment at 400 °C, for 10 h (b). Peaks marked with * and ° correspond to Li_3VO_4 and $LiVO_3$ phases, respectively.

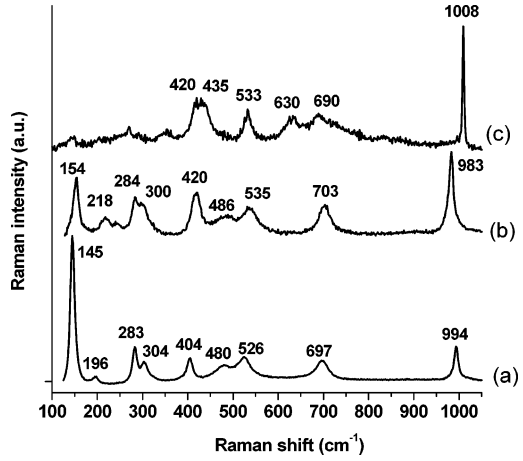

Figure 4. Raman spectra obtained for α-V_2O_5: (a) chemically prepared ϵ-$Li_{0.52}V_2O_5$ (b) and δ-LiV_2O_5 (c).

Table 2. Wavenumbers (in cm^{-1}) of Raman Active Modes Observed for the α-, ϵ-, and δ-Phases of $Li_xV_2O_5$ Samples[a]

α-V_2O_5	ϵ-$Li_{0.52}V_2O_5$	δ-LiV_2O_5
145vs	154s	145vw
196vw	218w	
283s	284m	271vw
304s	300m	355vw
404s	420s	420s
480m	486w	435s
526s	535m	533s
		630m
697s	703s	690m
		837vw
994s	983s	1008vs

[a] vs, very strong; s, strong; m, medium; w, weak; and vw: very weak.

(Figure 3b) exhibits the typical fingerprint of a well-crystallized γ-LiV_2O_5 (space group *Pnma*, $a = 9.68$ Å, $b = 3.60$ Å, and $c = 10.66$ Å), however, in a mixture with Li_3VO_4 and $LiVO_3$, as shown by the presence of new diffraction peaks.

Figure 4 shows the Raman spectra of the chemically prepared ϵ-$Li_{0.52}V_2O_5$ and δ-LiV_2O_5 powders compared to that of α-V_2O_5. The Raman wavenumbers of the corresponding phases are summarized in Table 2. Polarized Raman spectra for the V_2O_5 crystal have been previously studied.[32] The point symmetry group is D_{2h}, and the Raman features of crystalline V_2O_5 are composed of nine peaks at about 145, 196, 283, 304, 404, 480, 526, 697, and 994 cm^{-1} (Figure 4a). Most of the low-frequency modes can be described in terms of external modes of V_2O_5 units. They have been derived from relative motions of two V_2O_5 units belonging to the unit cell, two of them generating translational modes at 145 and 196 cm^{-1}. Internal modes, on the other hand, which are observed in the medium- and high-frequency region, can be described in terms of O−V−O and V−O−V bending modes and V−O stretching modes. The band at 994 cm^{-1} is assigned to the stretching vibration mode of the shortest $V-O_1$ bond directed along the *c* axis. The strong intensity of the translational mode located at 145 cm^{-1} reflects the long range order in the plane of the V_2O_5 sheets.

The Raman spectrum recorded for ϵ-$Li_{0.52}V_2O_5$ (see Table 2 and Figure 4b) exhibits several spectroscopic changes: the intensity of the translational mode is strongly quenched, and its wavenumber is shifted from 145 to 154 cm^{-1}. Several modes in the 200−700 cm^{-1} range are also shifted toward higher wavenumber: 196 to 218 cm^{-1}, 404 to 420 cm^{-1}, 480 to 486 cm^{-1}, 526 to 535 cm^{-1}, and 697 to 703 cm^{-1}. Conversely, the V═O stretching mode along the *c* axis decreases in frequency from 994 to 983 cm^{-1}. This shift in frequency has been shown to be consistent with the lengthening of the V═O bond from 1.58 Å for the α-phase to 1.6 Å for the ϵ-phase.[29]

The Raman spectrum of δ-LiV_2O_5 shown in Figure 4c can also be compared with that of α-V_2O_5 shown in Figure 4a. The low intensity of the bands in the low-frequency part of the Raman spectrum lines as well as the broadening of the bands overall in the spectrum of the δ-phase indicates that this phase is less ordered than the α- and ϵ-lattices. It is seen also that the same sole line, corresponding to the V═O stretching mode along the *c* axis, dominates in the high-frequency part of both spectra. In the spectrum of the δ-phase, this line is narrow and shifted up to 1008 cm^{-1} with respect to 994 cm^{-1} typical for the α-phase. This line can serve as a spectral fingerprint of the δ-phase. Other marked distinctions of the Raman spectrum of this phase are the presence of the peak at 630 cm^{-1} and the disappearance of the peak at 480 cm^{-1}.

The Raman features of the δ-phase reflect the particularity of this structure. As shown in Figure 2, the O1−O1 distances in the δ-phase (2.77 Å) are markedly shorter than in the α- and ϵ-phases (3 Å). It was suggested that the relatively high wavenumber of the V═O stretching mode is a spectroscopic manifestation of the steric V═O repulsion which becomes very strong in the δ-phase because of pronounced layer puckering.[33]

Figure 5a shows the Raman spectrum of the LR sample. The low intensity and broadness of the signal reflects the low crystallinity of the phase prepared at room temperature. A further annealing treatment at 400 °C (Figure 5b) allows the raw powder to crystallize, as shown by the emergence of new and well-resolved Raman features at 149, 173, 200, 222, 274, 279, 297, 329, 378, 435, 524, 548, 648, 735, 881, 945, 965, and 989 cm^{-1}. However, secondary phases are

(32) Abello, L.; Husson, E.; Repelin, Y.; Lucazeau, G. *Spectrochim. Acta* **1983**, *39A*, 641.
(33) Lassegues, J.-C. Private communication.

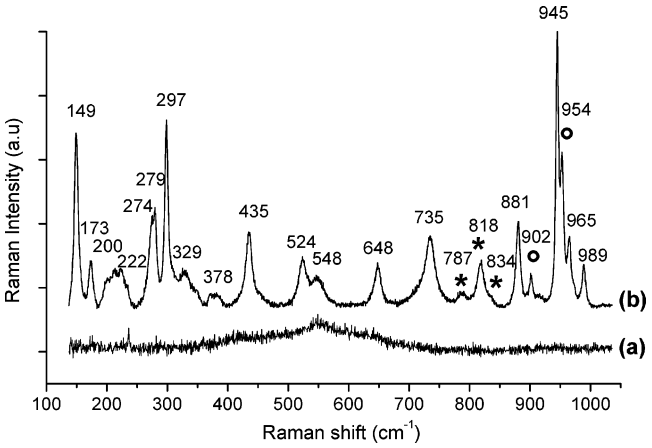

Figure 5. Raman spectra of the chemically prepared LR phase (a) and after annealing treatment at 400 °C, 10 h (b). Peaks marked with * and ° correspond to Li_3VO_4 and $LiVO_3$ phases, respectively.

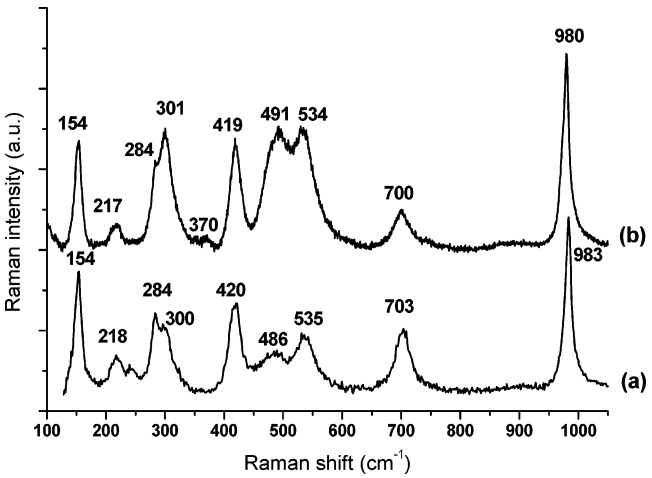

Figure 6. Raman spectra of chemical ϵ-$Li_{0.52}V_2O_5$ powder (a) and that previously reported for the electrochemical ϵ-$Li_{0.4}V_2O_5$ film[29] (b).

locally detected through the presence of characteristic Raman lines at 787, 818, and 834 cm^{-1} and 902 and 954 cm^{-1} assigned to Li_3VO_4 and $LiVO_3$ traces, respectively.

The following conclusions can be drawn from these spectroscopic data. First, as shown in Figure 6, the Raman spectrum of the chemical ϵ-$Li_{0.52}V_2O_5$ phase is in good agreement with that previously found for the electrochemically formed ϵ-$Li_{0.4}V_2O_5$ film.[29] Concerning the δ-LiV_2O_5 phase, the Raman fingerprint of the chemically prepared powder (Figure 7a) exhibits some disparities compared to that previously reported for the electrochemically lithiated δ-$Li_{0.9}V_2O_5$ film[29] (Figure 7b). In particular, the characteristic Raman features at 630 and 1008 cm^{-1} are not detected for the electrochemically formed compound which exhibits a Raman spectrum very close to that of the ϵ-phase, however, with a wavenumber value for the V═O stretching mode shifted down to 970 cm^{-1}.

We believe that the spectrum recorded for the chemically lithiated powder, using a very weak laser power ($I = 200$ μW; Figure 7a), corresponds to a "pure" δ-phase not affected by temperature-induced distortions. To confirm this assignment, Raman spectra have been recorded with progressive increase of the laser power and time exposure (see Figure 8). For a laser power of $I = 600$ μW (Figure 8b), new Raman bands appear at 973 cm^{-1} and in the low-frequency region

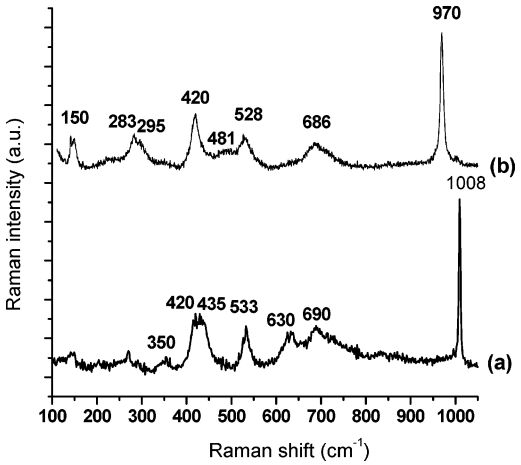

Figure 7. Raman spectra of chemical δ-LiV_2O_5 powder (a) and that previously reported for an electrochemical δ-$Li_{0.9}V_2O_5$ film[29] (b).

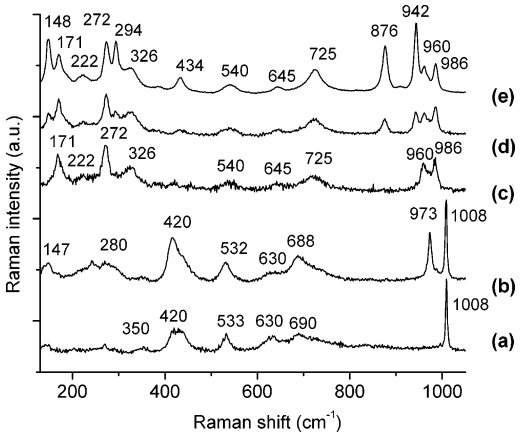

Figure 8. Raman spectra of chemical δ-LiV_2O_5 powder illuminated with a laser power of 0.2 mW (a), a laser power of 0.6 mW (b), a laser power of 0.8 mW and integration time of 20 s (c), a laser power of 0.8 mW and integration time of 90 s (d), and a laser power of 0.8 mW and integration time of 900 s (e).

(147−280 cm^{-1}) whereas the 1008 and 631 cm^{-1} characteristic lines of the δ-phase decrease in intensity. This spectral evolution corresponds to the transformation under the laser beam of the δ-LiV_2O_5 phase into the lithium rich ϵ-LiV_2O_5 phase. Indeed, the features observed for the Raman spectrum reported in Figure 8b are very close to those exhibited by the electrochemical δ-$Li_{0.9}V_2O_5$ spectrum reported in Figure 7b, which suggests that the thin film material has evolved under the laser beam.

For higher laser power ($I = 800$ μW, see Figure 8c), the 420 cm^{-1} line of the ϵ-phase disappears whereas new features are observed at 986, 960, 725, 645, 540, 326, 272, 222, and 171 cm^{-1}. These characteristic bands are kept on further increase of the sample exposition to the laser beam, with, however, several new lines which emerge at 942, 876, 434, 294, and 148 cm^{-1} (Figure 8d,e). The intensity of the new band at 876 cm^{-1} rapidly increases along with the increase of the radiation power. Such results clearly demonstrate that the δ-LiV_2O_5 compound is very sensitive to the power of the incident radiation. This peculiarity originates from the great metastability of the δ-LiV_2O_5 phase with respect to the $\delta-\epsilon-\gamma$ transformations. Indeed, it has been previously reported that for Li concentration $x = 1$, three $Li_xV_2O_5$ phases are found across the entire temperature range from room

Table 3. Wavenumbers (in cm^{-1}) of Raman Active Modes Observed for Various $Li_xV_2O_5$ Samples

γ-LiV_2O_5 single crystal[34]	γ-$Li_{0.95}V_2O_5$ powder[26]	δ-$Li_{0.95}V_2O_5$ powder[26]	γ-laser induced powder [this work]	γ_{LR} powder [this work]	γ_{th} powder [this work]	α-V_2O_5
168	154		148	149	145	145
172, 197	171	171	171	174, 200	**171**, **197**	**196**
209, 250	222	222	222	211, 222	209	
267, 270	276	274	272	274, 279	**271**, **282**	**283**
328, 333	296, 331	331	294, 326	299, 330	**301**, **327**	**304**
374	380	380		377	376	
398					404	404
456	434	419	434	435	482	480
528				524	528	526
546, 550	543	522	540	548	546	
639, 646	652	643	645	648	647	
725, 737	730	730	725	734	**703**, **737**	**697**
	876		876	880	881	
	942	942	942	945	947	
965	960, 972	960	960	966	966	
989	984	984	986	989	**992**, **997**	**994**

temperature up to 650 °C. Thermal energy allows first the $[V_2O_5]$ layers of the δ-phase to be rearranged and to produce the ϵ-phase at about 120 °C, after which around 350 °C the ϵ-phase tranforms into the γ-phase.[10]

It can be suggested that such drastic Raman changes reflect the structural variation in course of the $\delta-\gamma$ transformation. At illumination higher than 200 μW, the laser beam radiation heats the sample enough to induce in situ the $\delta-\epsilon-\gamma$ phase transitions. It is worth mentioning that the Raman spectrum reported by Zhang and Frech[26] for the chemically prepared δ-$Li_{0.95}V_2O_5$ phase exhibits striking similarity with that of the laser induced γ-LiV_2O_5 form (see Table 3 and Figure 8e). In particular, for this δ-reported phase,[26] a wide spectral structure consisting of four lines in the high wavenumber range emerges in place of the single line at 1008 cm^{-1}. These observations suggest that the Raman spectrum attributed to δ-$Li_{0.95}V_2O_5$ in ref 26 may rather be assigned to a laser induced γ-form produced under the laser beam.

Concerning the chemically prepared LR sample, both Raman and XRD data show the presence of side products, namely, Li_3VO_4 and $LiVO_3$. Such a result is consistent with previous data reported in the composition range $1 < x < 3$.[13] On the other hand, the Raman features of the main phase obtained in mixture with the vanadate species (see Figure 5 and Table 3) can be safely assigned to the γ fingerprint as they compare exactly with those of the laser induced γ-form (see Figure 8e and Table 3).

With the aim to obtain the Raman spectrum of the "pure" γ-LiV_2O_5 phase, we have studied the series of "high temperature" phase transitions $\delta \rightarrow \epsilon \rightarrow \gamma$ through the thermal behavior of δ-LiV_2O_5.

Structural Study of the $\delta \rightarrow \epsilon \rightarrow \gamma$ "High Temperature" Phase Transitions. The evolution of the XRD patterns of δ-LiV_2O_5 heat-treated at different temperatures in the 100−250 °C temperature range are reported in Figure 9a. An enlarged view in the 15−21 °C 2θ range is reported in Figure 9b.

At 100 °C the XRD pattern is typical of the δ-phase with unit cell parameters unchanged compared to the room-temperature compound. We observe, however, the emergence of a shoulder at ~19.30° (2θ) which could be ascribed to the most intense peak of the ϵ-phase (ϵ-001). At 135 °C, the intensity of the main diffraction line δ-002 decreases. At the same time the δ-200 and δ-102 peaks are broader because of the overlapping with respectively the ϵ-200 and ϵ-001 peaks. At 170 °C the ϵ-200 and ϵ-001 peaks are well-

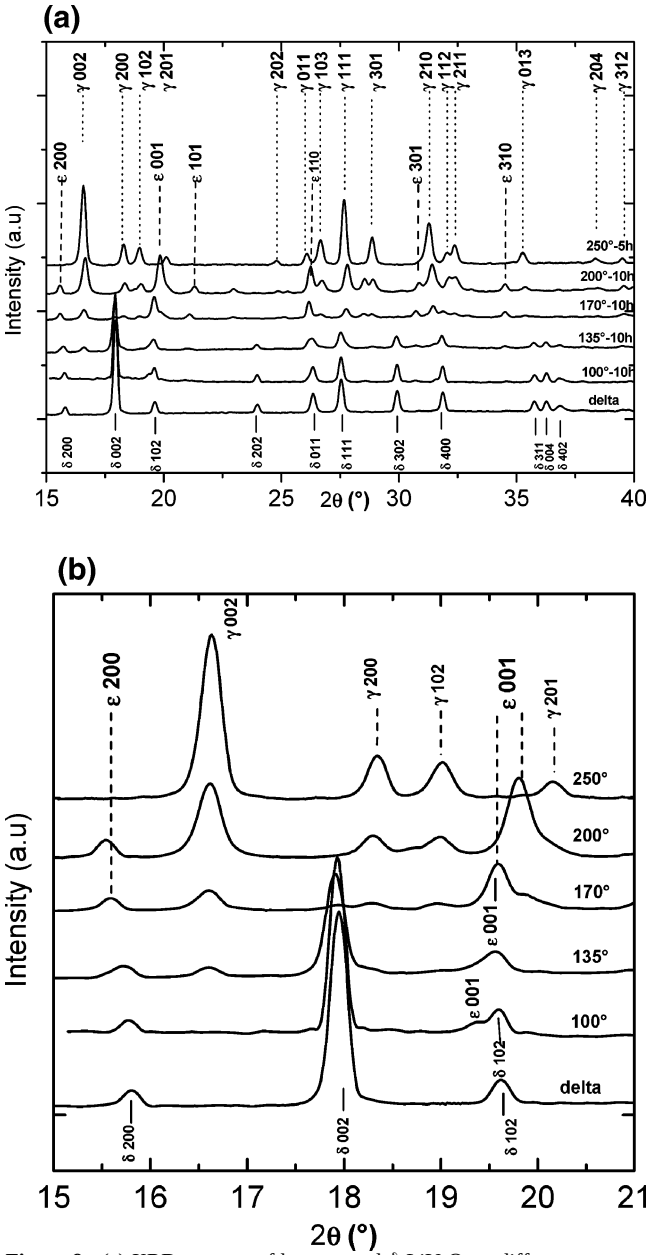

Figure 9. (a) XRD patterns of heat-treated δ-LiV_2O_5 at different temperatures. (b) Enlarged plot of the XRD patterns of heat-treated δ-LiV_2O_5 at different temperatures.

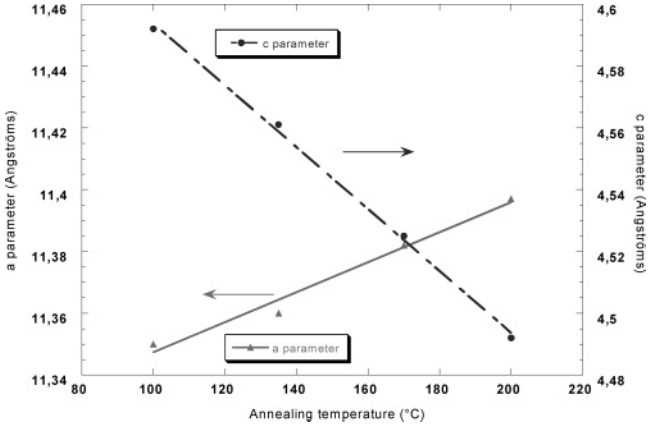

Figure 10. Unit cell parameters evolution as a function of the temperature for the high temperature ϵ-phase.

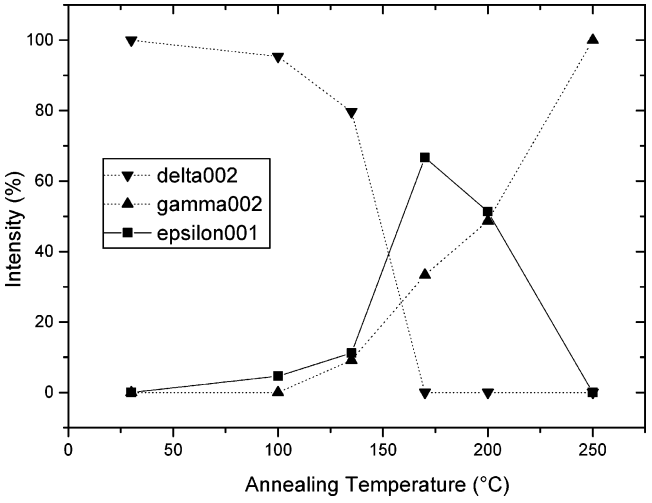

Figure 11. Intensity variations of the main peaks of the δ-, ϵ-, and γ_{th}-LiV_2O_5 phases.

distinguished, and at the same time, the γ-002 line increases in intensity at the expense of the δ-002 peak which has practically disappeared. At 200 °C, the XRD pattern is still composed of ϵ- and γ-*hkl* lines whereas at 250 °C it is exclusively indexed on the basis of the γ-phase (namely, γ_{th}) with the following unit cell parameters: $a = 9.69$ Å, $b = 3.60$ Å, and $c = 10.67$ Å.

Concerning the ϵ-phase, several shifts in angles are observed as a function of the temperature (Figure 9b). They correspond to changes in unit cell parameters reported in Figure 10. At 100 °C, a value of 4.59 Å for the *c* parameter can be extracted from the position of the ϵ-001 shoulder at ~19.30° (2θ). This peak shifts progressively toward higher angles: from 19.30° (2θ) at 100 °C to 19.48° (2θ) at 135 °C and 19.76° (2θ) at 200 °C. This evolution corresponds to a linear decrease in the *c* parameter from 4.59 Å at 100 °C to 4.49 Å at 200 °C. On the other hand, the shift of the ϵ-200 peak toward lower angles indicates a slight increase in the *a* parameter. As far as the γ-LiV_2O_5 phase is concerned, only a slight decrease in the *a* parameter is observed from 9.72 to 9.69 Å between 170 °C and 250 °C, the *b* and *c* parameters remaining constant within this temperature range.

The temperature evolution for the intensity of the main peak of each phase (δ_{002}, ϵ_{001}, and γ_{002}) is reported in Figure

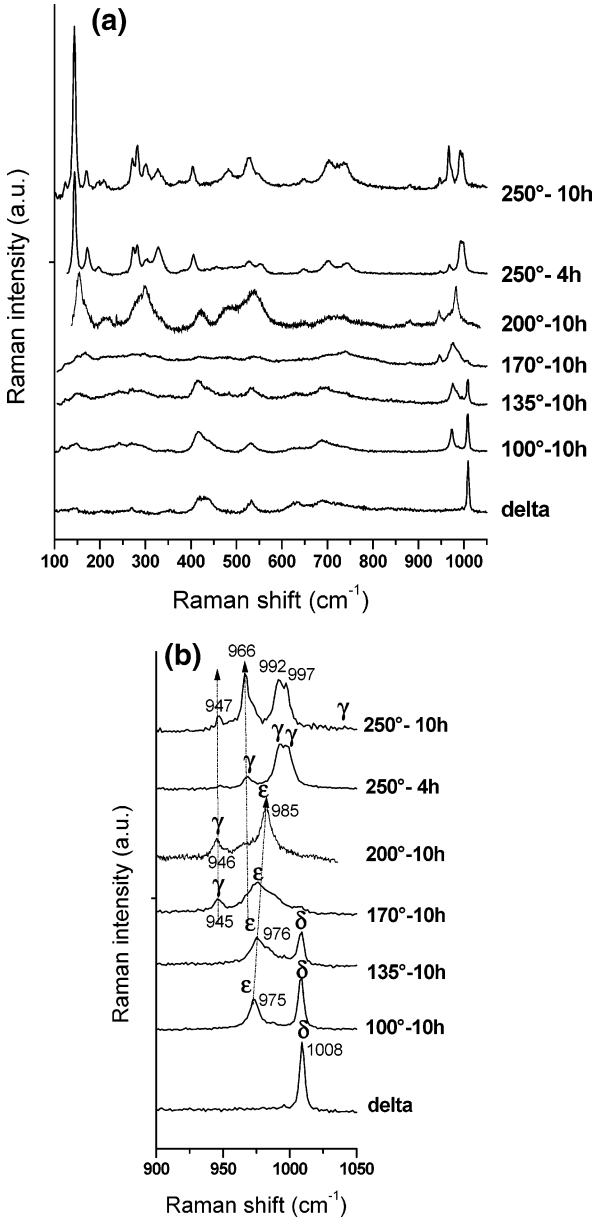

Figure 12. (a) Raman spectra of heat-treated δ-LiV_2O_5 at different temperatures. (b) Enlarged plot of the Raman spectra of heat-treated δ-LiV_2O_5 at different temperatures.

11. It comes out that $\delta \rightarrow \epsilon$ phase transition is initiated around 100 °C and the $\epsilon \rightarrow \gamma$ transformation proceeds from 135 °C. The $\delta \rightarrow \epsilon$ transformation ends at 170 °C, the ϵ- and γ-phases being simultaneously present. Finally, at 250 °C, the complete transformation of ϵ into γ-LiV_2O_5 is achieved. Such results are consistent with those recently reported using the Synchrotron X-ray powder analysis.[30]

The evolution of the Raman spectrum of δ-LiV_2O_5 heat-treated at different temperatures in the 100−250 °C temperature range is reported in Figure 12a. Besides the emergence of high-frequency bands, other characteristic frequency lines located in the 100−800 cm^{-1} range gradually appear, located at 145, 171, 271, 282, 301, 327, 404, 482, 528, 647, 703, and 737 cm^{-1}. Such strong spectral changes reveal the structural variation induced by the thermal treatment. In the low-frequency range, they may also reflect some strong electron−phonon interactions for in-plane lattice modes. An enlarged view of the high wavenumber region is

given in Figure 12b. It can be seen that the $\delta \rightarrow \epsilon$ transformation begins from 100 °C, as indicated by the emergence of the high-frequency band at 975 cm^{-1}. Up to 170 °C, both δ- and ϵ-phases coexist, the ϵ-phase growing at the expense of the δ-phase. At this temperature, the nucleation of the γ-phase begins, as pointed out by the appearance of a new feature at 945 cm^{-1}. At 200 °C, the Raman spectrum changes drastically with the emergence of intense and well-resolved Raman features in the whole wavenumber range indicating the crystallization of the γ-LiV_2O_5 phase. The $\epsilon \rightarrow \gamma$ transformation ends at 250 °C, as shown by the disappearance of the 985 cm^{-1} band. The characteristic Raman lines of the resulting γ_{th}-LiV_2O_5 phase are reported in Table 3.

The shift of the vanadyl stretching mode observed for the ϵ-phase (from 975 cm^{-1} at 100 °C to 985 cm^{-1} at 200 °C) indicates a strengthening of this bond, which is well-consistent with the decrease in the *c* parameter deduced from XRD experiments (Figure 10). The observed evolution and in particular the decrease in the *c* parameter with the temperature suggest that the high temperature ϵ-phase may release a fraction of Li ions between 100 °C and 200 °C. Furthermore, it has not been possible in our annealing conditions to isolate the pure ϵ-phase of stoichiometric LiV_2O_5 for which parameters in the range 11.33/11.36 Å, 3.57/3.59 Å, and 4.65/4.68 Å have been previously proposed.[1,10,30] It is clear that kinetics plays a major role in these transformations and that a slower heating rate should allow the temperature range of the two phase regions to be decreased.

Hence, the thermal treatment of the δ-phase at 250 °C allows the pure γ-phase LiV_2O_5, namely, γ_{th}-LiV_2O_5, to be obtained with the following lattice parameters: $a = 9.69$ Å, $b = 3.60$ Å, and $c = 10.67$ Å. Such values are in good agreement with the structural data previously reported by Galy et al. for γ-LiV_2O_5.[8,10] The space group of the γ-LiV_2O_5 structure is *Pnma* (D_{2h}^{16}). As in α− and δ-phases, this structure still contains the V_2O_5 layers perpendicular to the *z* axis, and the layers are built up of VO_2 ladders connected by V−O−V bridges. Likewise, in δ-phase, the layers are alternatively shifted on the vector *b*/2, and the unit cell of this structure is doubled in the *z* direction. The *xz* projection of this structure is shown in Figure 2d. However, the structure of the γ-phase differs from the structure of the δ-phase markedly. The Li atoms are shifted in the *x* direction from their symmetric positions in the δ-phase. This is accompanied by important deformations of the V_2O_5 layers. Each second ladder undergoes a strong transformation: it rotates along the *y* axis, and the O atoms of neighboring vinylic groups exchange their positions. These displacements are shown by curved arrows. As a result of such a deformation, two nonequivalent V positions (labeled as V1 and V2) appear, and the V1−O3−V2 bridges become strongly nonsymmetric. The same notations O1 and O2 are used in Figure 2d for oxygen atoms within nontransformed ladders with V1 atoms. Corresponding oxygen atoms within transformed ladders (with V2 atoms) are labeled as O1′ and O2′.

The Raman wavenumbers of the various γ-LiV_2O_5 compounds here synthesized, chemically prepared (γ_{LR}), laser induced from δ-LiV_2O_5, and thermally formed from δ-LiV_2O_5 (γ_{th}) are summarized in Table 3. Raman wavenumbers previously reported for γ-LiV_2O_5 single crystals[34] and γ-$Li_{0.95}V_2O_5$ powder[26] are also shown for comparison. It can be seen that, except for a few deviations, all prominent Raman features observed for the different γ powders are in good agreement with those measured for the single crystal. Considering the Raman features of the pure γ_{th}-LiV_2O_5, two weak lines at 881 and 947 cm^{-1} are observed, which were not detected in the spectrum of the single crystal. Furthermore, on comparing the Raman spectrum of γ_{th}-LiV_2O_5 (Figure 13) with that observed for α-V_2O_5 (Figure 4a), the following considerations can be observed: first, all main spectral features observed in α-V_2O_5 can be clearly discriminated in the spectrum of γ_{th}-LiV_2O_5 (see also Table 3). Second, some bands which have a singlet form in the Raman spectrum of α-, ϵ-, and δ-V_2O_5 are clearly twofold split in the spectrum of γ_{th}-LiV_2O_5 (see, in Table 3, wavenumber values in bold). Third, some new spectral features not seen in the Raman spectrum of α-V_2O_5 can be detected in the spectrum of γ_{th}-LiV_2O_5 (bands at 376, 546, 647, and 966 cm^{-1}). At least two factors can account for the distinction between the spectra of these crystals. First, the nonequivalent character of the ladders in the lattice of γ_{th}-LiV_2O_5, inducing two kinds of vanadium environments, must lead to the twofold splitting. Second, the Li atom oscillations may couple with some modes of the V_2O_5 lattice. Our lattice dynamics calculations actually in progress confirm this suggestion, especially for the high-frequency modes.[35]

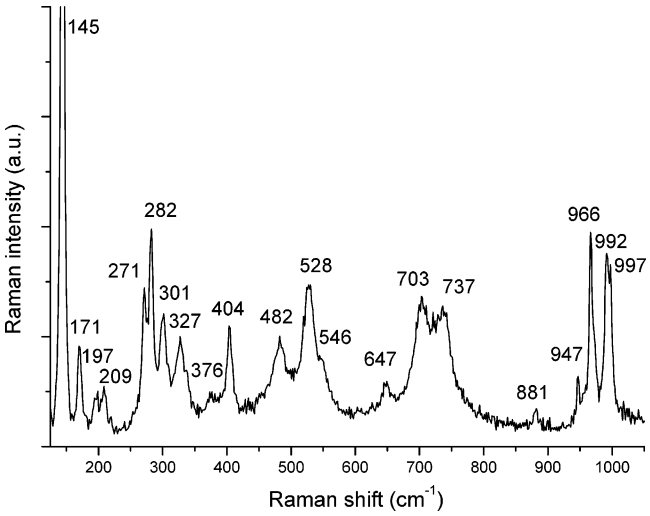

Figure 13. Raman spectrum of γ_{th}-LiV_2O_5.

Conclusions

The detailed Raman spectra of the ϵ-$Li_{0.52}V_2O_5$, δ-LiV_2O_5, and γ-LiV_2O_5 chemically prepared powdered phases have been established. They are all involved in the Li insertion process governing the electrochemical behavior of the V_2O_5 positive electrode in secondary lithium batteries. Among other bands, the high-frequency band assigned to the

(34) Popovic, Z. V.; Gajic, R.; Konstantinovic, M. J.; Provoost, R.; Moshchalkov, V. V.; Vasil'ev, A. N.; Isobe, M.; Ueda, Y. *Phys. Rev. B* **2000**, *61*, 11454.
(35) Baddour-Hadjean, R.; Smirnov, M.; Pereira-Ramos, J. P. To be submitted.

stretching vibration mode of the V═O bond along the *c* axis can serve as a typical spectral fingerprint for each phase. This line is located at 994 cm^{-1} for α-V_2O_5 and shifts to 983 cm^{-1} for ϵ-$Li_{0.52}V_2O_5$ and to 1008 cm^{-1} for δ-LiV_2O_5. The structural characteristics of each phase explain such a finding.

The knowledge of the Raman features of the $Li_xV_2O_5$ system has been applied to the investigation of the thermal treatment of the δ-LiV_2O_5 up to 250 °C. The emergence of the ϵ- and γ-phases induced by the temperature increase has been shown to take place from 100 and 170 °C, respectively. At 250 °C, the $\epsilon \rightarrow \gamma$ transformation is quantitative, allowing a well-defined Raman spectrum for the γ-LiV_2O_5 phase to be obtained.

The main Raman features observed for the γ-LiV_2O_5 phase are found to be in good agreement with those measured for the single crystal. The strongly distorted structure of γ-LiV_2O_5 compared to the α-, ϵ-, and δ-phases and especially the presence of two kinds of vanadium environment induce a splitting of some single bands (196, 283, 304, 697, and 994 cm^{-1}) into two lines and the emergence of new vibrational modes (376, 546, 647, and 966 cm^{-1}). Contrary to the other lithiated phases, the γ-LiV_2O_5 compound exhibits a complex high-frequency region characterized by a multiplet (four bands) located between 947 and 997 cm^{-1}. These results are consistent with the Raman spectrum achieved for a chemically prepared lithium-rich sample corresponding to a mixture of γ-phase and lithium vanadates. In other respects, we have demonstrated that with the use of a laser power higher than 200 μW, the radiation provokes the in situ transformation of the δ-phase into the γ-phase. Therefore, a careful and rigorous experimental approach is needed to establish unambiguously the Raman features of lithium intercalated compounds. Lattice dynamics calculations are under progress to allow the assignment of the whole Raman spectra of the α-, ϵ-, δ-, and γ-phases.

CM060540G